

1 **Kinematics of footwall exhumation at oceanic**
2 **detachment faults: solid-block rotation and apparent**
3 **unbending**

4 **Dan Sandiford^{1,2}, Sascha Brune^{2,3}, Anne Glerum², John Naliboff⁴, Joanne M.**
5 **Whittaker¹**

6 ¹Institute for Marine and Antarctic Studies, University of Tasmania, Hobart, Tasmania, Australia, 7004

7 ²Helmholtz Centre Potsdam - German Research Centre for Geosciences (GFZ)

8 ³Institute of Geosciences, University of Potsdam, Potsdam, Germany

9 ⁴Department of Earth and Environmental Science, New Mexico Institute of Mining and Technology

10 **Key Points:**

- 11 • Numerical models of footwall exhumation show a significant component of solid-
12 block rotation
- 13 • Brittle footwall deformation away from the detachment fault is dominated by ‘ap-
14 parent unbending’
- 15 • ‘Unbending’ since curvature gets reduced, ‘apparent’ as the footwall is not bent
16 in the first place

Corresponding author: Dan Sandiford, dan.sandiford@utas.edu.au

Abstract

Seafloor spreading at slow rates can be accommodated on large-offset oceanic detachment faults (ODFs), that exhume lower crustal and mantle rocks in footwall domes termed oceanic core complexes (OCCs). Footwall rock experiences large rotation during exhumation, yet important aspects of the kinematics - particularly the relative roles of solid-block rotation and flexure - are not clearly understood. Using a high-resolution numerical model, we explore the exhumation kinematics in the footwall beneath an emergent ODF/OCC. A key feature of the models is that footwall motion is dominated by solid-block rotation, accommodated by the concave-down ODF. This is attributed to a system behaviour in which the accumulation of distributed plastic strain is minimized. A consequence of these kinematics is that curvature measured along the ODF is representative of a neutral stress configuration, rather than a 'bent' one. Instead, it is in the subsequent process of 'apparent unbending' that significant flexural stresses are developed in the model footwall. The brittle strain associated with apparent unbending is produced dominantly in extension, beneath the OCC, consistent with earthquake clustering observed in the Trans-Atlantic Geotraverse at the Mid-Atlantic Ridge.

1 Introduction

Slip accumulation on major normal faults, such as those bounding slow spreading ridges, induces rebound and flexure due to unloading within the axial rift (Spencer, 1984; Wernicke & Axen, 1988; Buck, 1988). The flexural deformation may itself produce brittle failure, representing a cascade of deformation from major to subsidiary fault systems. Slow seafloor spreading is often taken up by extension on large-offset asymmetric detachment faults (ODFs), which exhume lower crustal and mantle rocks in domal footwall exposures termed oceanic core complexes (OCCs) (e.g. Cannat (1993); Tucholke (1998)). This study is primarily concerned with the kinematic characteristics of exhumation, the resulting flexural stress and deformation patterns, and the expression of these dynamics in footwall seismicity.

Paleomagnetic inclination data show that footwall blocks in ODF systems undergo significant rotation, typically 50-80°, during exhumation; a process that is often termed rollover (Morris et al., 2009; MacLeod et al., 2011; Garcés & Gee, 2007). What remains unclear, however, is whether the kinematics of exhumation (which ultimately produce

48 these estimated rotations) tend to be dominated by footwall flexure (simple bending),
49 solid-block rotation, or perhaps more complicated internal deformation patterns like flex-
50 ural slip or vertical simple shear (e.g. Wernicke and Axen (1988)). While the kinemat-
51 ics of exhumation has not received a great deal of attention in ODF settings (cf. con-
52 tinental core-complexes e.g. Wernicke and Axen (1988); Axen and Hartley (1997)) a fre-
53 quent assumption is that flexure plays an important role in footwall exhumation (e.g.
54 (Tucholke, 1998; MacLeod et al., 2002; Parnell-Turner et al., 2017; Cannat et al., 2019)).

55 This assumption is true not only in regard to the developmental stage of detach-
56 ments, where regional flexural-isostatic rebound plays a role in rotating planar normal
57 faults to shallower dips (e.g. Buck (1988)), but also in mature settings, with significant
58 (10s km) fault offset. In this view rollover ‘flexes the brittle footwall, such that the up-
59 per part of the footwall block is under tension’ (Tucholke (1998)). Likewise, the detach-
60 ment fault itself is thought to ‘rotate by flexure to low angles’ (MacLeod et al., 2002).
61 Again, ridge-parallel faults that intersect OCCs are often depicted as normal faults re-
62 lated to the inferred flexural tension in the upper part of the footwall (Tucholke et al.,
63 1998; MacLeod et al., 2002, 2009; Escartín et al., 2017; Collins et al., 2012). The inferred
64 relationship between OCC/ODF curvature and footwall flexural stress is what we refer
65 to as an elastic plate model. Such a relationship is completely absent in the numerical
66 models we discuss.

67 Seismicity provides insight into stress and, particularly, deformation patterns in the
68 brittle lithosphere, and thereby a potential means of constraining kinematics of footwall
69 exhumation. Previous seismicity studies suggest that significant brittle deformation oc-
70 curs in detachment footwalls as part of exhumation (Demartin et al., 2007; Parnell-Turner
71 et al., 2017). Most records of seismicity in detachment footwalls are dominated by normal-
72 faulting mechanisms and are often attributed to the same far-field tectonic stresses re-
73 sponsible for sustaining the extensional plate boundary (Demartin et al., 2007; Collins
74 et al., 2012; Grevemeyer et al., 2013). Compressional seismicity has also been observed
75 in ODF footwalls, and it is this observation that has been argued to be diagnostic of flex-
76 ure within the elastic plate framework (Parnell-Turner et al., 2017). However, the iden-
77 tified compressional earthquakes also exhibit significant variability in the orientation of
78 the focal mechanism P-axes. This casts some doubt over whether such events are rep-
79 resentative of a ‘tectonic’ stress state arising from flexure in the detachment system.

80 In the study of Demartin et al. (2007), which investigated the Trans-Atlantic Geo-
81 traverse (TAG) detachment (located on the Mid-Atlantic Ridge at $\sim 26^\circ$ N), focal mech-
82 anisms constructed from footwall seismicity are closely aligned with the spreading di-
83 rection. The authors identified two distinct zones of seismic activity, one interpreted to
84 represent the curved trace of the active detachment fault, and a second locus about 8
85 km outboard of the detachment cluster, inferred to represent slip on antithetic faults.
86 However, a dynamic explanation for the occurrence of this prominent, spatially-offset zone
87 of deformation within the footwall remains elusive.

88 In this paper, we investigate the kinematics of footwall exhumation beneath an emer-
89 gent ODF/OCC system, focusing on results from high-resolution numerical models. In
90 these models, solid-block rotation plays a dominant role in the kinematics of footwall ex-
91 humation. Our analysis explores the implications for flexural stress and deformation pat-
92 terns in the system. In doing so, we provide a potential explanation for the seismicity
93 patterns in the TAG detachment, while questioning the tectonic origin for compressional
94 seismicity at the $13^\circ 20'$ N detachment (cf. Parnell-Turner et al. (2017)). Our model sug-
95 gests that flexural strain is an important component of the seismic moment produced
96 in detachment footwalls, however the spatial relationship between flexural strain and de-
97 tachment curvature is very different to that assumed in elastic plate models.

98 **2 Numerical experiments**

99 We model the evolution of an amagmatic ODF setting using the open-source finite
100 element code ASPECT version 2.2.0 (see Kronbichler et al. (2012); Heister et al. (2017);
101 Bangerth et al. (2020, 2020b)). To do so, we solve the incompressible Stokes and advection-
102 diffusion equations, in a 2-D domain, subject to boundary conditions on the tempera-
103 ture and velocity. The model is initialised with a thin lithosphere, defined by a transient
104 cooling profile with a thermal age of 0.5 Myr in the center of the domain. The domain
105 is 400 km wide and 100 km deep. The thermal profile ages outwardly in proportion to
106 the applied spreading rate of 2 cm/yr (full rate), which is representative for slow ocean
107 ridges in general and similar to the current spreading rate at the TAG detachment (\sim
108 2.5 cm/yr) (Müller et al., 2016). Uniform inflow at the bottom boundary balances the
109 outward flux of material at the side boundaries. The model has a free surface (Rose et
110 al., 2017), and a diffusion process is applied to the surface topography in order to coun-
111 teract strong mesh deformation. The model has a static, hierarchical mesh refinement

112 such that the quadrilateral elements in the cold, brittle part of the model have an edge
 113 length of 125 meters, while at the base of the domain the element length is 2 km.

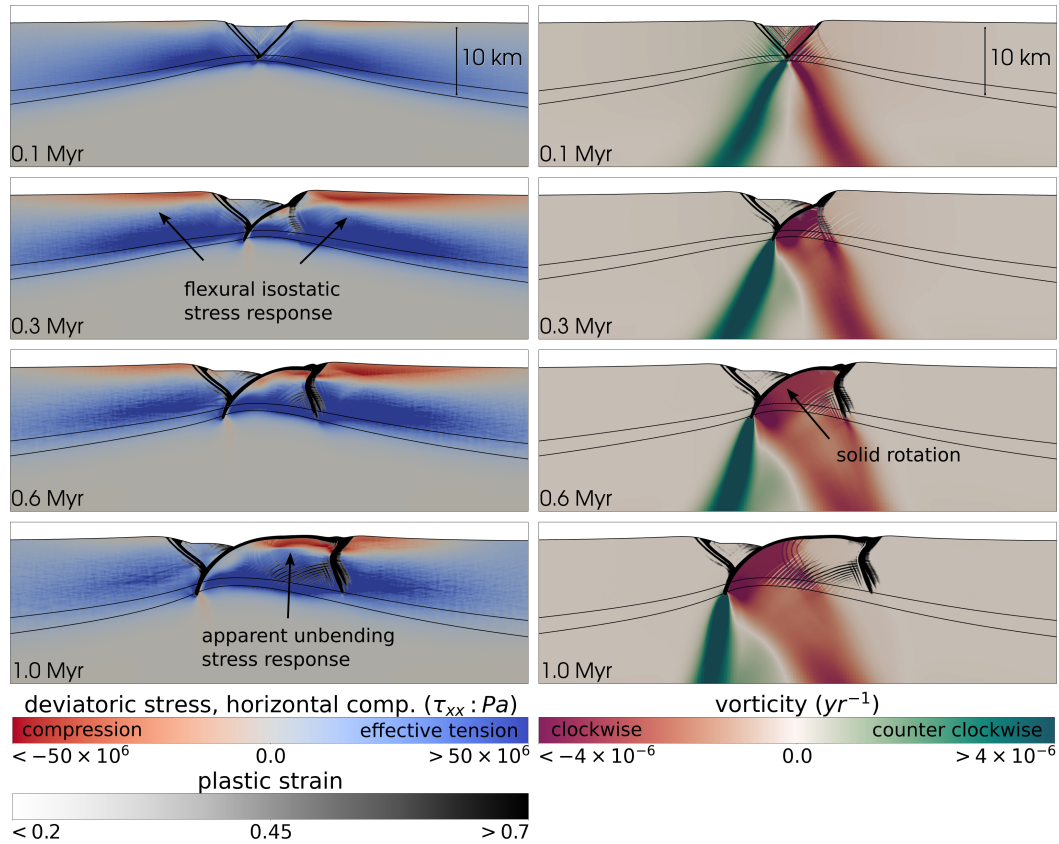


Figure 1. Evolution of reference numerical model from symmetric graben to asymmetric detachment system highlighting the role of solid-block rotation in exhumation as well as flexural processes. The left hand panels show horizontal component (τ_{xx}) of the deviatoric stress tensor, revealing flexural stress accumulation during the development of the ODF and footwall exhumation. The stress tensor definition, for the Maxwell visco-elastic plastic rheology, is discussed in the Supplementary Information. The right hand panels show the vorticity (counter-clockwise rotations are positive), and demonstrate the role of solid-block rotation in exhumation at various stages of the model evolution. The two black lines are contours of the temperature field at 600 and 700 °C. The accumulated plastic strain is shown with a transparent greyscale, showing the location of brittle structures. The full model evolution is animated in Supplementary movie S1.

114 There is no compositional differentiation in the model (i.e. no crust/mantle). All
 115 parts of the domain are subject to the same constitutive model. The constitutive model
 116 incorporates viscous (dislocation creep), elastic and plastic (pseudo-brittle) deformation

117 mechanisms, hereafter referred to as visco-elastic plastic (VEP) rheology, following the
118 approach of Moresi et al. (2003). The development and benchmarking of the rheolog-
119 ical model was guided by the study of Olive et al. (2016). The dominant deformation
120 mechanism is selected for each element based on the system state (temperature, stress,
121 accumulated strain). A random component of plastic strain is used to localise deforma-
122 tion. Further details and employed parameters are provided in the Supplementary in-
123 formation (Text S2, and Table S1). The ASPECT parameter file used to run the refer-
124 ence model can be downloaded from https://github.com/dansand/odf_paper, or from
125 the Supporting Information.

126 The development of detachment fault systems is associated with the existence of
127 faults that are significantly weaker than the host rock (Reston & Ranero, 2011), while
128 the additional development of rider blocks can depend on the relative amount of weak-
129 ening in the cohesion versus friction coefficient terms in the yield stress envelope (Choi
130 et al., 2013). Here, we applied weakening of the cohesion and friction angle as well as
131 of the prefactor in the dislocation creep law, similar to recent studies using ASPECT (Glerum
132 et al., 2018; Naliboff et al., 2020).

133 The reference model (e.g. Fig. 1) develops a large offset OCC (several 10s km), in
134 the absence of rider blocks (see Fig. 4 annotations for clarification) and remains stable
135 (quasi-steady state) for around 1 Myr, until the footwall breaks up and a new detach-
136 ment emerges. These timescale are consistent with the observed duration of individual
137 OCCs segments (Tucholke et al., 1998). In addition we present an alternative model (e.g.
138 Fig. 4) where the rate of plastic weakening is faster (cohesion/friction angle reduce lin-
139 early by factors of 0.5/0.1 over a strain interval of 2, rather than 6). In this model, the
140 footwall shows a greater tendency to break up, similar to previous modelling results (Lavie
141 et al., 2000).

142 **3 Model evolution, kinematics and deformation**

143 **3.1 Reference model evolution**

144 Figure 1 shows the evolution of the reference model from a brief stage of symmet-
145 rical necking through to a completely asymmetric ODF system. At 0.1 Myr, near-symmetric
146 planar faults are active, producing a graben with minor intra-rift faults. The load (deficit)
147 of the graben is supported through regional flexural-isostatic rebound, as revealed in the

148 horizontal component of the deviatoric stress tensor in the left hand panels of Fig. 1. This
 149 is one of two modes of lithospheric flexure exhibited by the model, as discussed later.

150 At 0.3 Myr the flexural-isostatic response has deformed the active faults, with the
 151 deeper parts of each conjugate fault becoming concave-down. At around this point, the
 152 model rapidly transitions to asymmetric extension. The right hand fault begins to sole
 153 into a wider zone of ductile shear at depth (the brittle-ductile transition occurs between
 154 the 600 and 700 °C temperature contours, shown with thin black lines in all Figures).
 155 Meanwhile the conjugate fault is abandoned. At this point, the flow of mantle material
 156 into the footwall of the active fault develops a strong solid-block rotation component (as
 157 shown in the vorticity field, right hand panels Fig. 1).

158 Beyond 0.3 Myr, slip along the detachment fault leads to the progressive up-dip
 159 migration of the breakaway zone, and exposure of the OCC (refer to annotations in Fig.
 160 2 as a guide to terminology). Between $\sim 1.0 - 2.0$ Myr, the geometry and kinematics of
 161 ODF/OCC system reaches quasi-steady state. After about 2.4 Myr, the footwall begins
 162 to break up, with an antithetic footwall fault becoming the locus for a new, oppositely-
 163 dipping, detachment. This stage of the model development is shown in the Supplemen-
 164 tary movie S1.

165 The early evolution of the ODF in our model shares some important similarities
 166 with the flexural rotation model (Buck, 1988). The load produced by the extension (the
 167 graben) is accommodated regionally through lithospheric flexure, which in turn deforms
 168 the normal fault, initiating a transition from planar fault to concave-down detachment.
 169 What is also evident in the numerical model is: a) the way in which detachment fault
 170 concavity is closely tied to the development of a rotational flow in the footwall (e.g. Fig.
 171 1 right hand panels); and b) the fact that this rotational flow initiates at depths just be-
 172 neath the brittle-ductile transition. The development of strong solid-block rotation oc-
 173 curs relatively early in the model evolution (~ 0.3 Myr). We describe this rotational com-
 174 ponent of exhumation in more detail in the following section.

175 **3.2 Exhumation kinematics**

176 Figure 2 shows features of the reference model after 1.5 Myr of evolution, with the
 177 ODF system in quasi-steady state (in the hanging wall reference frame). In the top panel
 178 of Fig. 2, we depict the square root of second invariant (hereafter magnitude) of the strain

179 rate tensor as well as the model velocity vectors. In the bottom panel of Fig. 2, we show
180 the flow vorticity as well as vectors of the translated velocity field (velocity in the hang-
181 ing wall reference frame).

182 In the footwall directly beneath the ODF, the combination of relatively high vor-
183 ticity and low strain rate magnitude indicates flow dominated by solid-block rotation.
184 This rotation is accommodated by the morphology of the active ODF, which approxi-
185 mates a circular arc through much of its active extent. Note that the zone of high vor-
186 ticity in the footwall extends slightly deeper than the base of the ODF. As we explain
187 in the Discussion, this provides the explanation for why the footwall does not exhibit the
188 stress state anticipated in the elastic stress model (i.e. tension in the upper-most part
189 of the footwall, with compression at greater depths).

190 With solid-block rotation dominant in the footwall beneath the ODF, and rigid plate
191 motion occurring in the outboard region (i.e, towards the right hand side of the model),
192 it follows that there must be a transitional zone between these flow regimes. In the ref-
193 erence model, this transition occurs as a zone of flexural deformation outboard from the
194 active ODF, beneath the OCC. The flexural nature of the deformation is revealed by the
195 polarised pattern in the horizontal deformation rate (Fig. 3, top panel) with shorten-
196 ing in the upper few kilometers and a significantly larger, triangular zone of active ex-
197 tension in the deeper part of the footwall.

198 We refer to this zone of flexural deformation as the zone of ‘apparent unbending’.
199 ‘Unbending’ because the flexural strain (change in curvature) is essentially measurable
200 by the straightening of the ODF, ‘apparent’ because the ODF footwall in our model is
201 not really bent in the first place. In other words, apparent unbending is a stress-accumulating
202 rather than a stress-releasing process, in contrast to the elastic plate model. The spa-
203 tial relationships between the zone of apparent unbending and ODF curvature is cov-
204 ered in more detail in the Discussion Section.

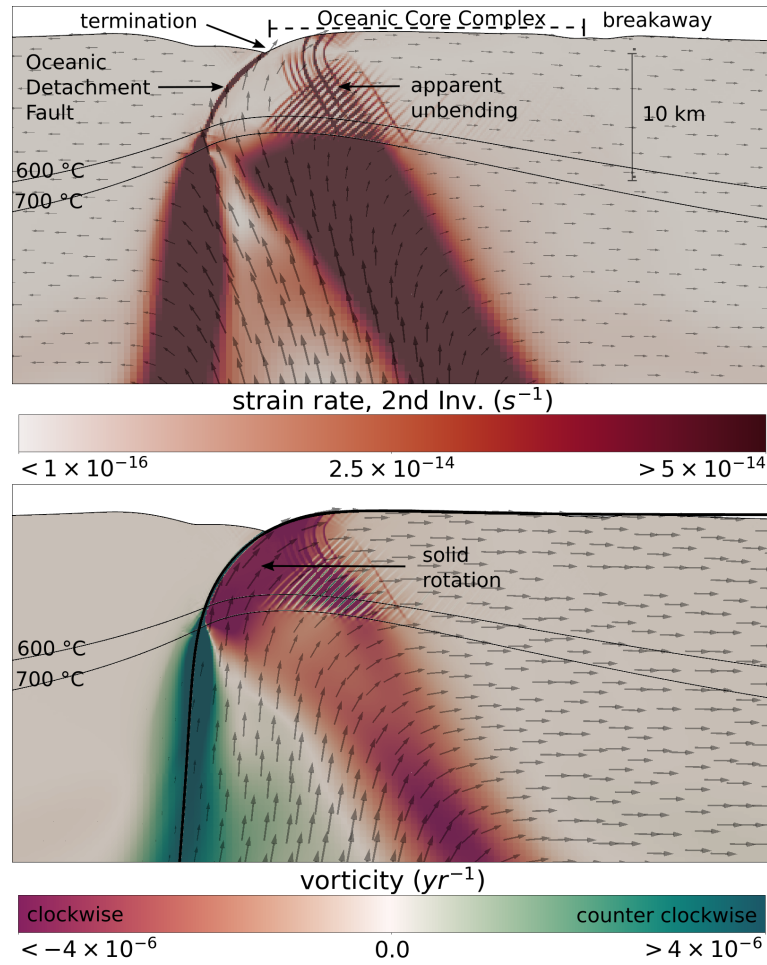


Figure 2. Reference model in quasi-steady state configuration, showing deformation localisation in the footwall outboard from the termination (apparent unbending), and solid-block rotation in the footwall beneath the ODF. Annotations show key features of the detachment system referred to in main text. The top panel shows the magnitude of the strain rate tensor: $|D| = (D_{ij}D_{ij})^{1/2}$; model velocity shown with arrows. Black lines are temperature contours shown at 600 and 700 °C, within which the brittle-ductile transition occurs. The bottom panel shows the flow vorticity; arrows show the velocity in the hanging wall reference frame (in which the system is quasi-steady state). The bold black line following the ODF/OCC is a parameterisation of the detachment geometry, undertaken in post-processing.

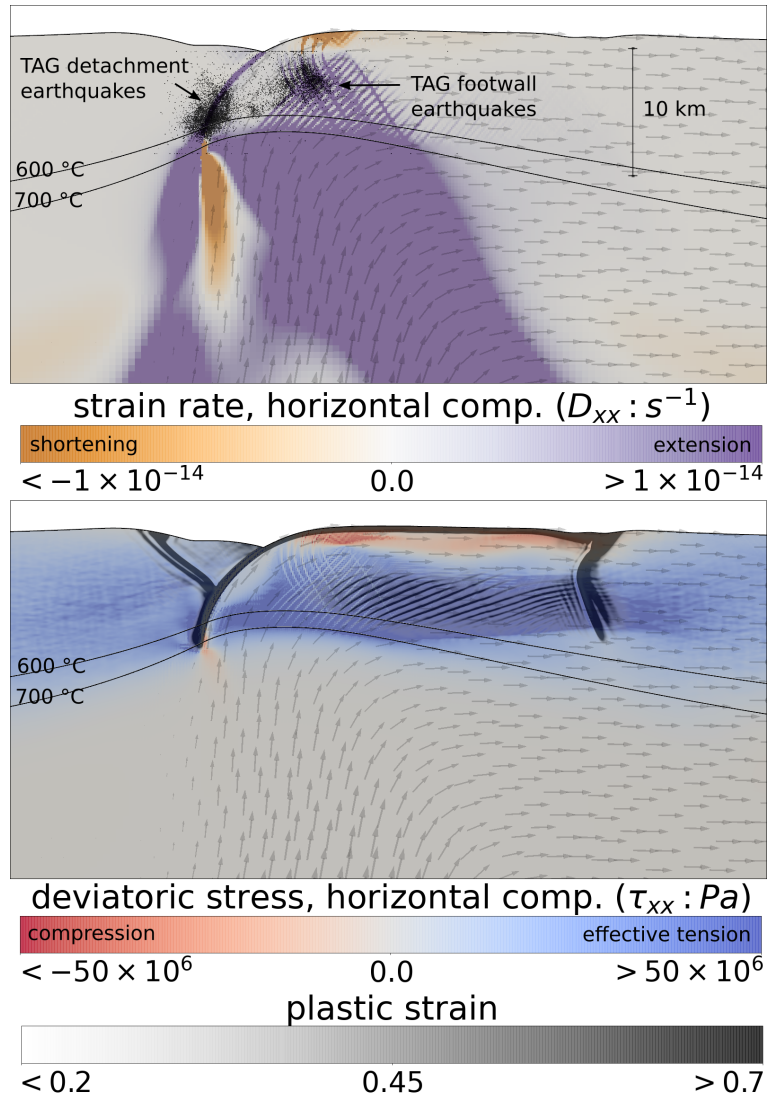


Figure 3. Reference model in quasi-steady state configuration at an elapsed time of 1.5 Myr, showing the strongly localised deformation rates associated with apparent unbending, as well as the stresses developed. Seismicity from the TAG segment is overlain as black dots (from Demartin et al. (2007)). The top panel shows the horizontal component (D_{xx}) of the strain rate tensor. The bottom panel shows the same component of the deviatoric stress tensor. Black lines show temperature contours at 600 and 700 °C. Grey vectors in both panels show the velocity field in the hanging-wall frame of motion.

205 Figure 3 shows that while stress and strain rates generally share the same sign (are
206 mainly co-axial), deformation tends to be more localised, while the resulting stresses are
207 to an extent ‘locked in’ to the plate. This is an important observation for thinking about
208 how to interpret patterns of seismicity from a geodynamic perspective; i.e. should vari-
209 ations in seismic moment (or activity rate) be compared with patterns of differential stress
210 or rather strain rates (or a combination of both, e.g. the brittle dissipation)? Our in-
211 terpretative framework is motivated by Chapple and Forsyth (1979) who argue that seis-
212 micity should be viewed as the expression of strain in the brittle regime. In this view,
213 zones of high brittle strain rate, along with the orientation of deformation, are the most
214 relevant quantities to compare to earthquake observations.

215 **3.3 Effects of Rapid Strain Weakening**

216 Figure 4 shows strain rates and vorticity from an alternative model where the rate
217 of plastic weakening is faster (cohesion/friction angle reduce by factors of 0.5/0.1 over
218 a strain interval of 2, rather than 6). This precludes the development of large displace-
219 ment, quasi-steady state detachment systems. Rather we see more rapid reorganisations,
220 along with various modes of ‘rider block’ formation and footwall breakup. The model
221 evolution is shown in more detail in Supplementary Movie S2.

222 Although the alternative model displays greater structural complexity and tempo-
223 ral variability than the reference model the large-scale kinematics are still the same. Ex-
224 humation of the footwall is likewise associated with a strong component of solid-block
225 rotation, shown by high (negative) values in the right hand panels of Fig. 4.

226 In the previous section, we discussed the kinematic requirement that deformation
227 must take place between the exhumation region, where the footwall is dominated by solid-
228 block rotation, and the outboard region where the plate undergoes rigid translation. In
229 the reference model, this transition occurs through a process of brittle flexure, which we
230 term apparent unbending. The alternative model also undergoes periods when the tran-
231 sition occurs through apparent unbending (e.g. snapshots at 0.6, 2.2, and 2.7 Myr). How-
232 ever, the alternative model demonstrates that the kinematic transition can instead oc-
233 cur through slip on a single through-going normal fault. This pattern is shown in the
234 snapshot at 1.3 Myr.

At this point, the footwall does not ‘apparently unbend’ in a coherent (flexural) manner, but rather it undergoes rotation as an almost-rigid block, bounded by major faults at either end (one being the ODF). The fault at the outboard edge on the right hand side of the block has a concave-up geometry, as is required to accommodate the rotation, in a sense mirroring that of the ODF, and it becomes sub-vertical near its surface exposure. This mode of footwall transition has some similarities with the ‘subvertical simple shear’ model, arising from an analogous kinematic problem in the context of continental core complexes (Wernicke & Axen, 1988).

Two aspects of the system are notable at this stage (1.3 Myr in Fig. 4). First, the kinematic transition between rotation and translation is achieved without any shallow footwall shortening (unlike in the case of apparent unbending). Secondly, the footwall exposure (OCC) at this stage has a domal shape, where material is rotationally-overturned, such that the slope and velocity vector at the outboard edge of the OCC have a downwards component (velocity vectors are shown in Supplementary movie S2).

4 Discussion

There are two main focus points of our discussion. First we consider flexural processes in our numerical models in more detail, highlighting contrasts with existing models for the flexural stress in ODF systems. Second we compare the modelled patterns of brittle deformation with observations of seismicity.

4.1 Flexural processes in footwall exhumation

Strain rates and stresses in our numerical models suggest an important role for flexure in footwall exhumation. The main locus of flexure in the reference model (e.g. Fig. 3) occurs outboard from the ODF termination, associated with shortening in the upper few kilometers of the OCC/footwall and extension beneath the neutral plane. We describe this process as apparent unbending. This flexural pattern is very different from that expected based on an elastic plate model, which has commonly been invoked for the flexural stress state of the footwall. In this view, rollover “*flexes the brittle footwall, such that the upper part of the footwall block is under tension*” (Tucholke, 1998). Recently, the discovery of compressional earthquake focal mechanisms in an ODF footwall has been interpreted in terms of an elastic plate model (Parnell-Turner et al., 2017). To under-

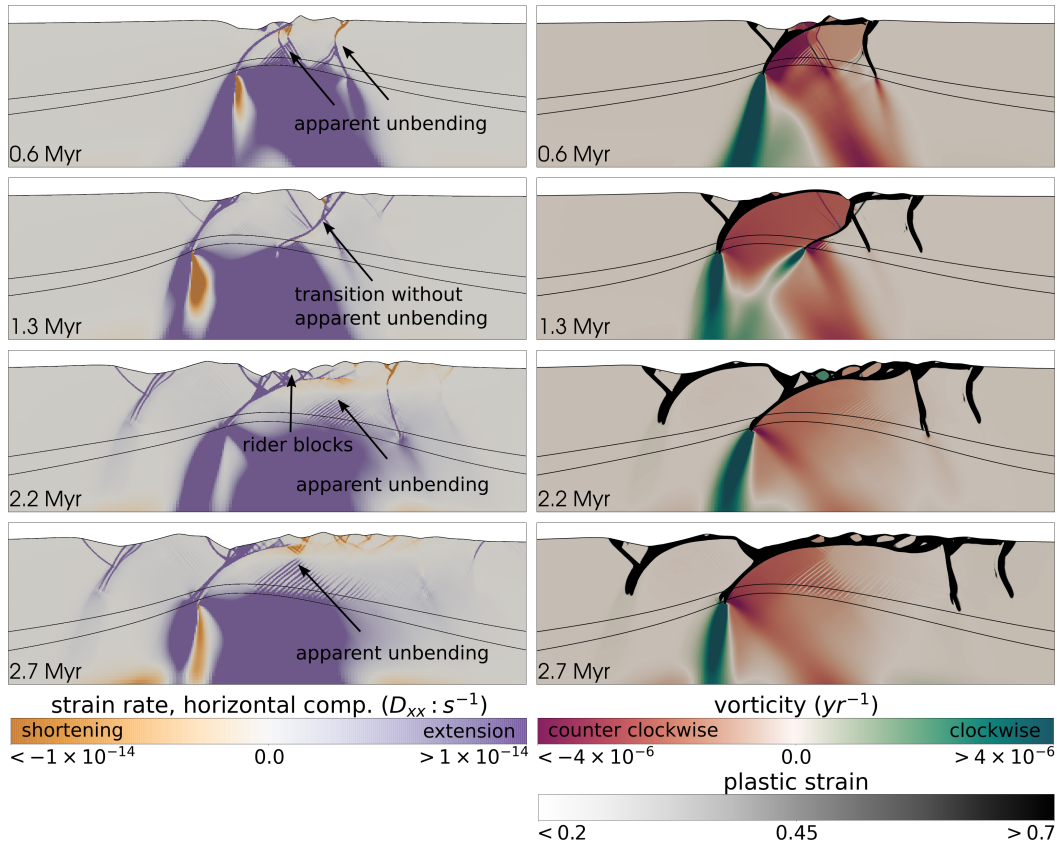


Figure 4. Evolution of model with more rapid strain weakening, showing the predominate role of solid-block rotation in the footwall beneath the ODF, though with greater structural complexity than the reference model. The left hand panels show the horizontal component (D_{xx}) of the strain rate tensor. The right hand panels show the vorticity, along with the accumulated plastic strain in greyscale. The two black lines are contours of the temperature field at 600 and 700 °C. The model evolution is shown in more detail in Supplementary Movie S2

stand the flexure patterns produced in our numerical models, and why these diverge from
 265 the expectation of an elastic plate model, we need to carefully consider both the mechan-
 266 ical and kinematic trajectory of the upwelling rock mass during exhumation.
 267

In Figure 1 and 3, we note that the magnitude of the deviatoric stress components
 268 increases dramatically at around 700 °C. The temperature range 600-700 °C marks the
 269 brittle-ductile transition (BDT) in the numerical model, which globally tends to define
 270 the limit of earthquake rupture in oceanic lithosphere (Jackson et al., 2008). In the case
 271 of our numerical model, the important point is that as upwelling footwall material crosses
 272 the BDT, the flow field is already dominated by a solid-block rotational component (Fig.
 273

274 2). Hence, there is no process of curvature increase (at least within the brittle-elastic regime)
275 to produce the stress state envisaged in an elastic plate model. How deformation is re-
276 solved beneath the BDT (in order for this rotational flow to develop) is of little conse-
277 quence, as the deviatoric stresses produced are negligible. In other words: rotation de-
278 velops before strength. It is for this reason that the ODF curvature is representative of
279 a neutral stress configuration, rather than a ‘bent’ one.

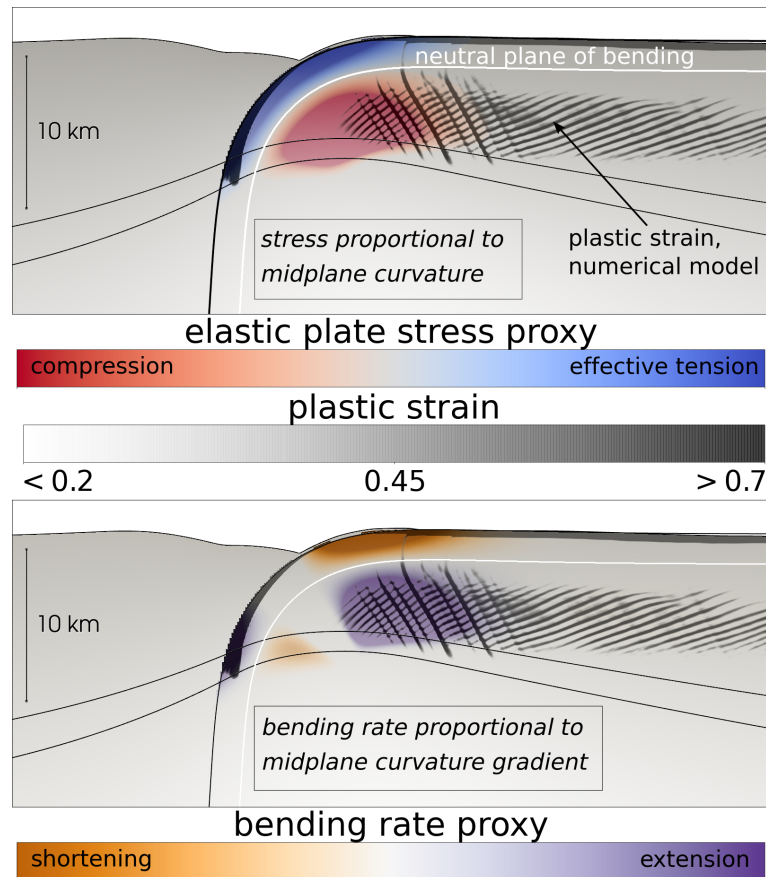


Figure 5. Contrast between an elastic plate relationship for footwall stress, based on the (static) curvature the ODF/OCC (top panel) and a kinematic view of exhumation, where apparent unbending is the dominant flexural process (bottom panel). A simple parameterisation of the detachment geometry (black line) provides the curvature (for the elastic plate relationship) and curvature gradient (for the advective bending rate relationship). In both panels, the white line represents the neutral plane of bending, positioned 2 km beneath the detachment surface, based on the location in our numerical model. All dynamic features (e.g. compression/shortening) are expressed relative to the neutral plane geometry. To generate the figure, the stress/bending rate magnitude was increased in proportion to the distance from the neutral plane, until reaching one of: a distance of 4 km, the detachment surface, or the 700 °C isotherm. At these points, the magnitude was rapidly tapered to zero. These are simply schematic representations designed to illustrate the differences between an elastic-plate view of stress (top panel, as discussed by Parnell-Turner et al. (2017), versus the flexural process that dominates our model (i.e. apparent unbending, bottom panel). In both figures the accumulated plastic strain from our reference numerical model is shown (at an elapsed time of 2.0 Myr) in transparent greyscale.

280 Moreover, once footwall material is exhumed beyond the zone of solid-block rota-
281 tion, flexure occurs, following the trend of decreasing curvature in the OCC outboard
282 of the detachment termination (i.e. apparent unbending). Counter-intuitively, material
283 in the footwall of our numerical model undergoes virtually monotonic flexural strain with
284 exactly the opposite polarity to that implied by the detachment curvature. These con-
285 trasts between an elastic plate model and the flexural bending rates that are associated
286 with apparent unbending are highlighted in Fig. 5.

287 An important aspect of apparent unbending is that flexural deformation is present
288 even when the morphology of the system is quasi-static. These strains arise because the
289 advective rate of curvature, which is proportional to curvature gradients (e.g. Fig. 5),
290 is non-zero (Kawakatsu, 1986; Sandiford et al., 2020). Apparent unbending is a kinematic,
291 rather than a flexural-isostatic process. Unlike the strain rates, the stress state in the
292 footwall (and hanging wall) will also remain influenced by the flexural-isostatic compen-
293 sation of the axial valley in a steady-state configuration.

294 While the alternative numerical model (Fig. 4) shows a more complex evolution,
295 exhumation is likewise dominated by solid-block rotation. Hence, the same general con-
296 clusions follow in regard to the fact that detachment curvature is a misleading proxy for
297 flexural stress.

298 To our knowledge, the process of apparent unbending has not been discussed in pre-
299 vious modelling studies nor its relationship to solid-block rotation in detachment foot-
300 walls. Yet a number of previous numerical models show strain rate patterns consistent
301 with this kinematic feature. Figures 2b&c of the 2d models of Tucholke et al. (2008) show
302 a zone of high strain rate outboard of the surface ODF exposure. The geometry of this
303 zone shows a characteristic triangular hourglass pattern, suggestive of flexural strain. A
304 similar feature can be discerned in the 3d models of Howell et al. (2019), although the
305 vertical exaggeration makes the pattern less clear. In both cases, only the magnitude of
306 the strain rate tensor is shown (rather than its horizontal components), so the flexural
307 nature of the deformation cannot be identified with complete confidence. Nevertheless,
308 it appears that the kinematic processes we have identified in our model are evident in
309 previous numerical modelling studies.

310 **4.2 Flexure and brittle deformation in models**

311 The accumulated plastic (pseudo-brittle) strain in the reference model is shown in
 312 Fig. 3 (at 1.5 Myr) and Fig. 5 (at 2.0 Myr). Comparing the zone of plastic strain ac-
 313 cumulation with the sign of stress or strain rate horizontal components (e.g. Fig. 3) re-
 314 veals that the plastic strain accumulated during exhumation is almost entirely generated
 315 by extensional-type structures in the region of apparent unbending. These patterns in
 316 the accumulated plastic strain show that while there is a flexural origin for most of the
 317 brittle strain in the detachment footwall, its seismic expression is expected to be dom-
 318 inated by normal faulting.

319 Earlier in the reference model development, footwall faulting is characterised by
 320 normal faults synthetic to the ODF (e.g Fig. 3 at 1.5 Myr). Later in the model, we see
 321 a systematic spatial trend where extension occurs on closely-spaced ODF-synthetic nor-
 322 mal faults nearer the axial valley, moving outboard to more widely spaced antithetic faults.
 323 Note how in Fig. 5, these larger antithetic faults can be seen to offset the fabric devel-
 324 oped by the synthetic-dipping faults. Ultimately, one of the major antithetic normal faults
 325 becomes the structure on which a new detachment fault forms, reversing the dip of the
 326 detachment (as is shown in Supplementary movie S1).

327 **4.3 Observational constraints and predictions**

328 In the previous sections we summarised kinematic and deformation patterns in our
 329 numerical models. We now discuss these patterns in connection to observations of seis-
 330 micity from ODF/OCC segments. Recording small magnitude events and obtaining pre-
 331 cise earthquake hypocenters in ODF regions generally requires hydrophone or ocean-bottom
 332 seismograph deployment. Hence, at this stage only a small number of pertinent stud-
 333 ies exist (Demartin et al., 2007; Parnell-Turner et al., 2017; Collins et al., 2012; Greve-
 334 meyer et al., 2013; Parnell-Turner et al., 2020). Even fewer show a pattern of hypocen-
 335 ters in which a dominant asymmetric detachment is convincingly delineated, which would
 336 suggest a tectonic configuration analogous to our model setup.

337 Supplementary Fig. S1 shows map and cross-sectional views of the hypocenters at
 338 the TAG detachment from Demartin et al. (2007). In Fig. 3, we plot a narrow swathe
 339 (those epicenters ≤ 4.5 km of the line shown in Fig. S1) of the TAG earthquakes over-
 340 laid on the horizontal strain rate component from our model. This exercise suggests that

341 important features of the TAG detachment seismicity can be explained by the kinematic
342 and flexural patterns we have discussed. In particular, the combination of solid-block ro-
343 tation beneath the detachment and apparent unbending beneath the OCC may explain
344 why the TAG footwall directly beneath the ODF has sparse seismicity, while extensional
345 seismicity is concentrated outboard of the termination. It can also explain why footwall
346 seismicity is concentrated at depths greater than ~ 2 km beneath the sea floor (see Fig.
347 S1 for location of seismicity relative to the TAG bathymetry).

348 Nevertheless, it is clear the footwall earthquake cluster imaged by Demartin et al.
349 (2007) is significantly more limited in its spatial extent than compared to the region of
350 high strain rates developed in the model (e.g. Fig 3). A few points are worth bearing
351 in mind, however: the seismic deployment detailed in Demartin et al. (2007) was rela-
352 tively short (eight months), and seismicity patterns may be biased with respect to the
353 long-term tectonic strain rates; there may be additional variability in terms of whether
354 faulting occurs as unstable sliding (e.g. earthquakes) versus stable slip (e.g. Mark et al.
355 (2018)), as well as the level of micro-seismicity versus larger events (i.e. the b-value). Sim-
356 ilarly, procedures on the numerical modelling side could be implicated: we omit phys-
357 ical processes such as melting, hydrothermal heat transport as well as any 3-dimensional
358 aspects of dynamics which may effect thermal and dynamic structure of the footwall. More-
359 over, the constitutive models utilised in our simulations, convergence of associated non-
360 linearity, and the implications of mesh sensitivity, are areas of active research, debate
361 and experimentation for the geodynamic discipline (e.g. Duretz et al. (2020)). It will there-
362 fore be important to explore whether the kinematic features we identify are equally promi-
363 nent in the models of other groups that use different numerical approaches, constitutive
364 models and physical approximations.

365 Our numerical models do not offer a ready explanation for compressional seismic-
366 ity directly beneath the ODF, as reported by Parnell-Turner et al. (2017). However, these
367 compressional earthquakes also exhibit significant variability in the orientation of the fo-
368 cal mechanism P-axes (unlike the cluster attributed to the detachment fault itself - Fig.
369 2C of that study). This is a potential indication that these earthquakes do not have a
370 tectonic origin, or at least that the causes for deformation cannot be reduced to 2d plane-
371 strain processes like elastic plate bending or apparent unbending. We note that in a follow-
372 up study of this region, which also encompasses areas directly to the north, the vivid clus-
373 ter of compressional events is completely absent (Parnell-Turner et al., 2020). Rather,

374 this later study mainly captures earthquakes inferred to belong to the detachment faults,
375 as well as streaks of activity outboard of the axial valley beneath the OCC/footwall. In
376 the 13°30'N detachment region, for instance, clustering is broadly comparable to the TAG
377 patterns, although event numbers are much smaller.

378 A prediction of our reference numerical model is that a small amount of shorten-
379 ing may occur in the shallowest few kilometers of OCCs, associated with the process of
380 apparent unbending. The steep thrust structures that accommodate this strain have a
381 total downdip extent of only a few kilometers, and they are expected to contribute a very
382 minor part of the total seismic moment associated with footwall exhumation (see the pat-
383 terns of accumulated plastic strain in Fig. 5). While such deformation may be difficult
384 to capture in the short term seismic record, these steeply-dipping reverse faults repre-
385 sent the active structures that should intersect exposed OCCs, in places where they tend
386 to flatten (curvature reduction) outboard of the detachment termination.

387 OCCs are known to be dissected by spreading-perpendicular faults, although there
388 is clearly much variability, such as observed at the adjacent Mid Atlantic Ridge detach-
389 ments at $\sim 13^\circ 20'$ N (no obvious dissecting faults) and $13^\circ 30'$ N (with dissecting faults),
390 e.g. Parnell-Turner et al. (2018). These structures are usually inferred to be normal faults
391 attributed to bending stresses during footwall rollover (Tucholke et al., 1998; Escartín
392 et al., 2003), i.e. invoking an elastic plate stress relationship.

393 The alternative numerical model shows that footwall rotation during exhumation
394 is not always associated with apparent unbending (i.e. Fig. 4 snapshot at 1.3 Myr). The
395 transition from rotation to rigid plate translation can instead occur via a major through-
396 going fault at the outboard edge of the block. Hence, our model results should not be
397 interpreted as suggesting that all OCC footwalls must undergo apparent unbending and
398 hence exhibit evidence of minor thrust faults. Rather, the key prediction of the models
399 is that exhumation beneath concave-down ODFs is dominated by solid-block rotation.
400 The zone of solid-block rotation must transition, via some pattern of deformation, to the
401 outboard region of rigid plate translation. Our models show two modes in which this may
402 occur. We suggest that where exposed OCCs reduce their curvature outboard of the ODF
403 termination, yet remain largely coherent, the flexure should be associated with short-
404 ening, compressional stress accumulation, and minor thrust faults.

5 Conclusions

This study addresses the nature of footwall exhumation in ODF settings, based on results of high-resolution numerical models. Exhumation is characterised by a strong component of solid-block rotation, accommodated by the concave-down ODF. This has important implications for how flexural processes operate in the system. We demonstrate a relationship between flexural stress and detachment curvature that is very different to the elastic plate model previously typically assumed. Our model also helps differentiate between the static flexural stress component associated with regional compensation of the axial depression, and a kinematic component of flexure associated with the transition from solid-block rotation of the footwall to rigid plate translation (apparent unbending).

Our results suggest that flexure related to apparent unbending may provide a significant component of the extensional seismic moment in detachment footwalls. Whereas Parnell-Turner et al. (2017) argued that bending may cause ‘compression in extension’, our models rather suggests that bending may promote ‘extension in extension’. The deformation patterns predicted in our model are broadly applicable to micro-seismicity patterns from the TAG detachment.

The geometry of detachment faults has classically been analysed from the perspective of fault mechanics and evolution, in which fault rotation and footwall rollover are associated with the flexural-isostatic response of the lithosphere to extension. Our model suggests that, while these processes are certainly important in the development of the detachment system, the system can evolve into a configuration that goes somewhat beyond the dynamics described in the flexural rotation model. In this configuration, the ODF geometry has a very specific relationship to the kinematics of exhumation, namely the accommodation of solid-block rotation of the footwall. The ODF in our models appears to be acting less as a classical fault and more in the sense of an exhumation channel (Brune et al., 2014). We speculate that minimization of distributed plastic strain may play a role in the ultimate geometric configuration of the ODF and the mechanics of exhumation; this provides one avenue for future research into these enigmatic plate boundary zones.

435 **Acknowledgments**

436 Figures were created using Pyvista, a Python interface for the Visualization Toolkit
 437 (VTK) (Sullivan & Kaszynski, 2019). DS, SB, and JMW were supported by Australian
 438 Research Council grant DP180102280. AG was supported by the Helmholtz Young In-
 439 vestigators Group CRYSTALS (grant no. VH-NG-1132). Data is available is available
 440 through Demartin et al. (2007) (10.1594/IEDA/306798).

441 **References**

- 442 Axen, G. J., & Hartley, J. M. (1997). Field tests of rolling hinges: Existence, me-
 443 chanical types, and implications for extensional tectonics. *Journal of Geophysi-
 444 cal Research: Solid Earth*, 102(B9), 20515–20537.
- 445 Bangerth, W., Dannberg, J., Gassmoeller, R., & Heister, T. (2020, June). *Aspect*
 446 *v2.2.0*. Zenodo. Retrieved from <https://doi.org/10.5281/zenodo.3924604>
 447 doi: 10.5281/zenodo.3924604
- 448 Bangerth, W., Dannberg, J., Gassm oller, R., Heister, T., et al. (2020b, June). AS-
 449 PECT: Advanced Solver for Problems in Earth’s ConvecTion, User Man-
 450 ual. Retrieved from <https://doi.org/10.6084/m9.figshare.4865333>
 451 (doi:10.6084/m9.figshare.4865333) doi: 10.6084/m9.figshare.4865333
- 452 Brune, S., Heine, C., P erez-Gussiny e, M., & Sobolev, S. V. (2014). Rift migra-
 453 tion explains continental margin asymmetry and crustal hyper-extension. *Na-
 454 ture communications*, 5(1), 1–9.
- 455 Buck, W. R. (1988). Flexural rotation of normal faults. *Tectonics*, 7(5), 959–973.
- 456 Cannat, M. (1993). Emplacement of mantle rocks in the seafloor at mid-ocean
 457 ridges. *Journal of Geophysical Research: Solid Earth*, 98(B3), 4163–4172.
- 458 Cannat, M., Sauter, D., Lavier, L., Bickert, M., Momoh, E., & Leroy, S. (2019). On
 459 spreading modes and magma supply at slow and ultraslow mid-ocean ridges.
 460 *Earth and Planetary Science Letters*, 519, 223–233.
- 461 Chapple, W. M., & Forsyth, D. W. (1979). Earthquakes and bending of plates at
 462 trenches. *Journal of Geophysical Research: Solid Earth*, 84(B12), 6729–6749.
- 463 Choi, E., Buck, W. R., Lavier, L. L., & Petersen, K. D. (2013). Using core complex
 464 geometry to constrain fault strength. *Geophysical Research Letters*, 40(15),
 465 3863–3867.
- 466 Collins, J. A., Smith, D. K., & McGuire, J. J. (2012). Seismicity of the atlantis

- 467 massif detachment fault, 30° n at the mid-atlantic ridge. *Geochemistry, Geo-*
468 *physics, Geosystems, 13(10).*
- 469 Demartin, B. J., Sohn, R. A., Canales, J. P., & Humphris, S. E. (2007). Kinematics
470 and geometry of active detachment faulting beneath the trans-atlantic geo-
471 traverse (tag) hydrothermal field on the mid-atlantic ridge. *Geology, 35(8),*
472 711–714.
- 473 Duretz, T., de Borst, R., Yamato, P., & Le Pourhiet, L. (2020). Toward robust and
474 predictive geodynamic modeling: The way forward in frictional plasticity. *Geo-*
475 *physical Research Letters, 47(5),* e2019GL086027.
- 476 Escartín, J., Mével, C., MacLeod, C. J., & McCaig, A. (2003). Constraints on de-
477 formation conditions and the origin of oceanic detachments: The mid-atlantic
478 ridge core complex at 15 45 n. *Geochemistry, Geophysics, Geosystems, 4(8).*
- 479 Escartín, J., Mevel, C., Petersen, S., Bonnemains, D., Cannat, M., Andreani, M., ...
480 others (2017). Tectonic structure, evolution, and the nature of oceanic core
481 complexes and their detachment fault zones (13 20 n and 13 30 n, mid atlantic
482 ridge). *Geochemistry, Geophysics, Geosystems, 18(4),* 1451–1482.
- 483 Garcés, M., & Gee, J. S. (2007). Paleomagnetic evidence of large footwall rotations
484 associated with low-angle faults at the mid-atlantic ridge. *Geology, 35(3),* 279–
485 282.
- 486 Glerum, A., Thieulot, C., Fraters, M., Blom, C., & Spakman, W. (2018). Nonlinear
487 viscoplasticity in aspect: benchmarking and applications to subduction. *Solid*
488 *Earth, 9,* 267–294.
- 489 Grevemeyer, I., Reston, T. J., & Moeller, S. (2013). Microseismicity of the mid-
490 atlantic ridge at 7° s–8° 15 s and at the logatchev massif oceanic core complex
491 at 14° 40 n–14° 50 n. *Geochemistry, Geophysics, Geosystems, 14(9),* 3532–
492 3554.
- 493 Heister, T., Dannberg, J., Gassmöller, R., & Bangerth, W. (2017). High accu-
494 racy mantle convection simulation through modern numerical methods. II:
495 Realistic models and problems. *Geophysical Journal International, 210(2),*
496 833–851. Retrieved from <https://doi.org/10.1093/gji/ggx195> doi:
497 10.1093/gji/ggx195
- 498 Howell, S. M., Olive, J.-A., Ito, G., Behn, M. D., Escartin, J., & Kaus, B. (2019).
499 Seafloor expression of oceanic detachment faulting reflects gradients in mid-

- 500 ocean ridge magma supply. *Earth and Planetary Science Letters*, 516, 176–
501 189.
- 502 Jackson, J., McKenzie, D., Priestley, K., & Emmerson, B. (2008). New views on
503 the structure and rheology of the lithosphere. *Journal of the Geological Soci-*
504 *ety*, 165(2), 453–465.
- 505 Kawakatsu, H. (1986). Double seismic zones: kinematics. *Journal of Geophysical Re-*
506 *search: Solid Earth*, 91(B5), 4811–4825.
- 507 Kronbichler, M., Heister, T., & Bangerth, W. (2012). High accuracy mantle convec-
508 tion simulation through modern numerical methods. *Geophysical Journal In-*
509 *ternational*, 191, 12–29. Retrieved from <http://dx.doi.org/10.1111/j.1365-246X.2012.05609.x>
510 doi: 10.1111/j.1365-246X.2012.05609.x
- 511 Lavier, L. L., Buck, W. R., & Poliakov, A. N. (2000). Factors controlling normal
512 fault offset in an ideal brittle layer. *Journal of Geophysical Research: Solid*
513 *Earth*, 105(B10), 23431–23442.
- 514 MacLeod, C. J., Carlut, J., Escartín, J., Horen, H., & Morris, A. (2011). Quanti-
515 tative constraint on footwall rotations at the 15° 45 n oceanic core complex,
516 mid-atlantic ridge: Implications for oceanic detachment fault processes. *Geo-*
517 *chemistry, Geophysics, Geosystems*, 12(5).
- 518 MacLeod, C. J., Escartin, J., Banerji, D., Banks, G., Gleeson, M., Irving, D. H. B.,
519 ... others (2002). Direct geological evidence for oceanic detachment faulting:
520 The mid-atlantic ridge, 15 45 n. *Geology*, 30(10), 879–882.
- 521 MacLeod, C. J., Searle, R., Murton, B., Casey, J., Mallows, C., Unsworth, S., ...
522 Harris, M. (2009). Life cycle of oceanic core complexes. *Earth and Planetary*
523 *Science Letters*, 287(3–4), 333–344.
- 524 Mark, H. F., Behn, M. D., Olive, J.-A., & Liu, Y. (2018). Controls on mid-ocean
525 ridge normal fault seismicity across spreading rates from rate-and-state friction
526 models. *Journal of Geophysical Research: Solid Earth*, 123(8), 6719–6733.
- 527 Moresi, L., Dufour, F., & Mühlhaus, H.-B. (2003). A lagrangian integration point
528 finite element method for large deformation modeling of viscoelastic geomateri-
529 als. *Journal of computational physics*, 184(2), 476–497.
- 530 Morris, A., Gee, J., Pressling, N., John, B., MacLeod, C. J., Grimes, C., & Searle,
531 R. (2009). Footwall rotation in an oceanic core complex quantified using re-
532 oriented integrated ocean drilling program core samples. *Earth and Planetary*

- 533 *Science Letters*, 287(1-2), 217–228.
- 534 Müller, R. D., Seton, M., Zahirovic, S., Williams, S. E., Matthews, K. J., Wright,
535 N. M., ... others (2016). Ocean basin evolution and global-scale plate reorga-
536 nization events since pangea breakup. *Annual Review of Earth and Planetary*
537 *Sciences*, 44, 107–138.
- 538 Naliboff, J., Glerum, A., Brune, S., Péron-Pinvidic, G., & Wrona, T. (2020). Devel-
539 opment of 3-d rift heterogeneity through fault network evolution. *Geophysical*
540 *Research Letters*, 47(13), e2019GL086611.
- 541 Olive, J.-A., Behn, M. D., Mittelstaedt, E., Ito, G., & Klein, B. Z. (2016). The
542 role of elasticity in simulating long-term tectonic extension. *Geophysical Jour-*
543 *nal International*, 205(2), 728–743.
- 544 Parnell-Turner, R., Escartin, J., Olive, J.-A., Smith, D. K., & Petersen, S. (2018).
545 Genesis of corrugated fault surfaces by strain localization recorded at oceanic
546 detachments. *Earth and Planetary Science Letters*, 498, 116–128.
- 547 Parnell-Turner, R., Sohn, R., Peirce, C., Reston, T., MacLeod, C., Searle, R., &
548 Simão, N. (2020). Seismicity trends and detachment fault structure at 13° n,
549 mid-atlantic ridge. *Geology*.
- 550 Parnell-Turner, R., Sohn, R., Peirce, C., Reston, T., MacLeod, C. J., Searle, R., &
551 Simão, N. (2017). Oceanic detachment faults generate compression in exten-
552 sion. *Geology*, 45(10), 923–926.
- 553 Reston, T., & Ranero, C. R. (2011). The 3-d geometry of detachment faulting at
554 mid-ocean ridges. *Geochemistry, Geophysics, Geosystems*, 12(7).
- 555 Rose, I., Buffett, B., & Heister, T. (2017). Stability and accuracy of free surface time
556 integration in viscous flows. *Physics of the Earth and Planetary Interiors*, 262,
557 90 - 100. Retrieved from <http://dx.doi.org/10.1016/j.pepi.2016.11.007>
558 doi: 10.1016/j.pepi.2016.11.007
- 559 Sandiford, D., Moresi, L. M., Sandiford, M., Farrington, R., & Yang, T. (2020). The
560 fingerprints of flexure in slab seismicity. *Tectonics*, 39(8), e2019TC005894.
- 561 Spencer, J. E. (1984). Role of tectonic denudation in warping and uplift of low-angle
562 normal faults. *Geology*, 12(2), 95–98.
- 563 Sullivan, C. B., & Kaszynski, A. (2019, may). PyVista: 3d plotting and mesh anal-
564 ysis through a streamlined interface for the visualization toolkit (VTK). *Jour-*
565 *nal of Open Source Software*, 4(37), 1450. Retrieved from <https://doi.org/>

566 10.21105/joss.01450 doi: 10.21105/joss.01450

567 Tucholke, B. E. (1998). Discovery of " megamullions" reveals gateways into the ocean
568 crust and upper mantle. *OCEANUS-WOODS HOLE MASS.*, 41, 15–19.

569 Tucholke, B. E., Behn, M. D., Buck, W. R., & Lin, J. (2008). Role of melt supply
570 in oceanic detachment faulting and formation of megamullions. *Geology*, 36(6),
571 455–458.

572 Tucholke, B. E., Lin, J., & Kleinrock, M. C. (1998). Megamullions and mullion
573 structure defining oceanic metamorphic core complexes on the mid-atlantic
574 ridge. *Journal of Geophysical Research: Solid Earth*, 103(B5), 9857–9866.

575 Wernicke, B., & Axen, G. J. (1988). On the role of isostasy in the evolution of nor-
576 mal fault systems. *Geology*, 16(9), 848–851.